

Cite this: *Chem. Sci.*, 2022, 13, 10082

All publication charges for this article have been paid for by the Royal Society of Chemistry

Received 21st May 2022

Accepted 18th July 2022

DOI: 10.1039/d2sc02852b

rsc.li/chemical-science

The smallest 4f-metalla-aromatic molecule of cyclo-PrB₂[−] with Pr–B multiple bonds†‡

Zhen-Ling Wang,^{§a} Teng-Teng Chen,^{§b} Wei-Jia Chen,^b Wan-Lu Li,^a Jing Zhao,^{Ⓜa} Xue-Lian Jiang,^c Jun Li,^{Ⓜc} Lai-Sheng Wang^{Ⓜ*b} and Han-Shi Hu^{Ⓜ*a}

The concept of metalla-aromaticity proposed by Thorn–Hoffmann (*Nouv. J. Chim.* 1979, 3, 39) has been expanded to organometallic molecules of transition metals that have more than one independent electron-delocalized system. Lanthanides, with highly contracted 4f atomic orbitals, are rarely found in multiply aromatic systems. Here we report the discovery of a doubly aromatic triatomic lanthanide-boron molecule PrB₂[−] based on a joint photoelectron spectroscopy and quantum chemical investigation. Global minimum structural searches reveal that PrB₂[−] has a C_{2v} triangular structure with a paramagnetic triplet ³B₂ electronic ground state, which can be viewed as featuring a trivalent Pr(III,f²) and B₂^{4−}. Chemical bonding analyses show that this cyclo-PrB₂[−] species is the smallest 4f-metalla-aromatic system exhibiting σ and π double aromaticity and multiple Pr–B bonding characters. It also sheds light on the formation of the rare B₂^{4−} tetraanion by the high-lying 5d orbitals of the 4f-elements, completing the isoelectronic B₂^{4−}, C₂^{2−}, N₂, and O₂²⁺ series.

1 Introduction

The concept of aromaticity and its role in stabilizing molecules, clusters and materials have been well developed in chemistry. Classical aromaticity usually refers to delocalized (p-p)π systems in unsaturated cyclic hydrocarbons such as benzene. In recent years, the concept of multiple aromaticity has been developed, which involves multiple independent delocalized electron systems (σ, π, δ, or even φ) coexisting in the same molecular systems. The first molecule with σ + π double aromaticity was observed in C₆H₃⁺ in 1979.¹ In the same year, a seminal paper by Thorn and Hoffmann² introduced transition metals into the field of aromaticity, which broadened the scope of this subject into “metalla-aromatic chemistry”. In this scenario, a carbon atom of an aromatic hydrocarbon is substituted by a transition metal atom, such that the bonding situation changes into a (d-p)π system. Since then, numerous transition metal compounds with metalla-aromaticity have been synthesized.^{3,4} Additionally,

many metal clusters have been found to be multiply aromatic, e.g., Mo₃S₄⁴⁺, Al₄^{2−}, Li₃⁺, Hg₄^{6−}, Ta₃O₃[−], Hf₃, and U₄(NH)₄.^{5–16} However, organolanthanide systems with metalla-aromaticity are rare because the 5d orbitals of lanthanides are energetically too high, while the 4f orbitals are radially too contracted to participate in effective bonding with carbon-based ligands.

Compared with its carbon neighbour, the electron-deficient boron element possesses higher 2p-orbital energy and larger 2s-2p orbital radii than carbon,^{17,18} which favours efficient bonding with energetically high-lying 5d orbitals of lanthanides, as exemplified by a number of lanthanide boride materials.¹⁹ Joint photoelectron spectroscopy (PES) and quantum chemical studies have shown that size-selected anionic boron clusters (B_n[−]) are planar or quasi-planar up to B₃₈[−].²⁰ All the planar boron clusters feature multi-centre delocalized σ and π bonds over the boron plane, which is a direct consequence of boron's electron efficiency.^{21–25} These delocalized σ and π bonds give rise to multiple aromaticity, which stabilizes the planar structures and leads to the concept of all-boron analogues (e.g. borophene) of polycyclic aromatic hydrocarbons.²³ Metal-doped boron clusters have recently become a new direction in the study of boron chemistry. It has been discovered that transition metals can be doped into the plane of boron clusters due to the strong metal–boron bonding.^{26–28} The d AOs of transition metals are found to participate in electron delocalization in doped planar boron clusters, resulting in the discovery of aromatic metal-centred borometallic wheels, M@B_n[−] (n = 8–10).^{29–34} Very recently, it has been shown that the Re atom can be

^aDepartment of Chemistry & Key Laboratory of Organic Optoelectronics and Molecular Engineering of the Ministry of Education, Tsinghua University, Beijing, 100084, China. E-mail: hshu@mail.tsinghua.edu.cn

^bDepartment of Chemistry, Brown University, Providence 02912, Rhode Island, USA. E-mail: Lai-Sheng_Wang@brown.edu

^cDepartment of Chemistry, Southern University of Science and Technology, Shenzhen 518055, China

† Dedicated to Professor Dr W. H. E. Schwarz on his 85th birthday.

‡ Electronic supplementary information (ESI) available. See <https://doi.org/10.1039/d2sc02852b>

§ These authors contributed equally to this work.



Table 1 The experimental VDEs for PrB_2^- ($^3\text{B}_2$) compared with computational values using the $\Delta\text{SCF-TDDFT}$ method at the level of SAOP/TZP using ADF code

	VDE (eV) (expt.)	VDE (eV) (comput.) ^a	State	Configuration ^{b,c}
PrB_2^-			$^3\text{B}_2$	$\{\dots 4a_1^2 3b_2^2 2b_1^2 [5a_1^{\uparrow} 4b_2^{\uparrow}] 5a_1^{\downarrow} 6a_1^{\uparrow} 7a_1^{\uparrow} 6a_1^{\downarrow}\}$
X	1.72	1.72	$^4\text{B}_2$	$\{\dots 4a_1^2 3b_2^2 2b_1^2 [5a_1^{\uparrow} 4b_2^{\uparrow}] 5a_1^{\downarrow} 6a_1^{\uparrow} 7a_1^{\uparrow} 6a_1^0\}$
A	1.90	1.95	$^4\text{B}_2$	$\{\dots 4a_1^2 3b_2^2 2b_1^2 [5a_1^{\uparrow} 4b_2^{\uparrow}] 5a_1^0 6a_1^{\uparrow} 7a_1^{\uparrow} 6a_1^{\downarrow}\}$
		1.98	$^2\text{B}_2$	$\{\dots 4a_1^2 3b_2^2 2b_1^2 [5a_1^{\uparrow} 4b_2^{\uparrow}] 5a_1^{\downarrow} 6a_1^{\uparrow} 7a_1^0 6a_1^{\downarrow}\}$
		2.05	$^2\text{B}_2$	$\{\dots 4a_1^2 3b_2^2 2b_1^2 [5a_1^{\uparrow} 4b_2^{\uparrow}] 5a_1^{\downarrow} 6a_1^0 7a_1^{\uparrow} 6a_1^{\downarrow}\}$
B	2.29	2.42	$^4\text{A}_2$	$\{\dots 4a_1^2 3b_2^2 2b_1^{\uparrow} [5a_1^{\uparrow} 4b_2^{\uparrow}] 5a_1^{\downarrow} 6a_1^{\uparrow} 7a_1^{\uparrow} 6a_1^{\downarrow}\}$
		2.64	$^2\text{A}_2$	$\{\dots 4a_1^2 3b_2^2 2b_1^{\downarrow} [5a_1^{\uparrow} 4b_2^{\uparrow}] 5a_1^{\downarrow} 6a_1^{\uparrow} 7a_1^{\uparrow} 6a_1^{\downarrow}\}$
C	3.13	2.98	$^2\text{B}_2$	$\{\dots 4a_1^2 3b_2^2 2b_1^2 [5a_1^0 4b_2^{\uparrow}] 5a_1^{\downarrow} 6a_1^{\uparrow} 7a_1^{\uparrow} 6a_1^{\downarrow}\}$
		3.07	$^2\text{A}_1$	$\{\dots 4a_1^2 3b_2^2 2b_1^2 [5a_1^{\uparrow} 4b_2^0] 5a_1^{\downarrow} 6a_1^{\uparrow} 7a_1^{\uparrow} 6a_1^{\downarrow}\}$
D	~3.9	3.72	$^4\text{A}_1$	$\{\dots 4a_1^2 3b_2^{\uparrow} 2b_1^2 [5a_1^{\uparrow} 4b_2^{\uparrow}] 5a_1^{\downarrow} 6a_1^{\uparrow} 7a_1^{\uparrow} 6a_1^{\downarrow}\}$
		3.88	$^2\text{A}_1$	$\{\dots 4a_1^2 3b_2^{\downarrow} 2b_1^2 [5a_1^{\uparrow} 4b_2^{\uparrow}] 5a_1^{\downarrow} 6a_1^{\uparrow} 7a_1^{\uparrow} 6a_1^{\downarrow}\}$

^a The calculated VDEs at the level of SAOP/TZP (at the PBE0 geometry) using ADF code are systematically shifted up by 0.20 eV to align calculated VDE₁ value with band X. ^b “ \uparrow ” and “ \downarrow ” in the electron configurations stand for α and β electrons, respectively. ^c The α -MOs $5a_1$ and $4b_2$ mainly arise from quasi-atomic Pr(III, f^2) configuration.

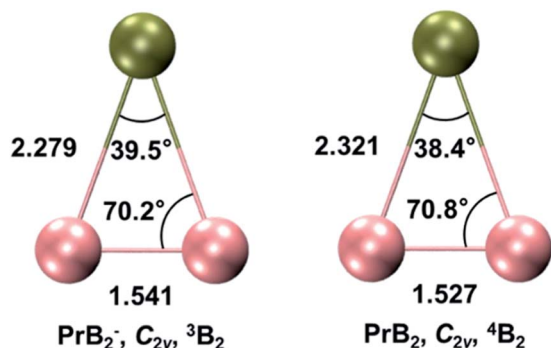


Fig. 2 The global minimum structures of PrB_2^- and PrB_2 calculated at the PBE0/TZP level using ADF program. The bond lengths are given in Å and the bond angles are given in degree ($^\circ$). Colour codes for atoms: olive-Pr; pink - B.

B-B $2p\sigma$ MO and the vertical (π_{\perp}) and horizontal (π_{\parallel}) B-B $2p\pi$ MOs, which all interact with $6s$ or $5d$ orbitals of Pr in an in-plane or out-of-plane fashion (Fig. 4). These bands have relatively high intensities due to the large detachment cross sections of the B $2p$ orbitals. The fact that the $6a_1\beta$ and $5a_1\beta$ electrons are detached before $7a_1\alpha$ and $6a_1\alpha$ is due to the favoured exchange interaction with the paramagnetic, quasi-atomic Pr f^2 configuration. Detachments of the $4f$ electrons in the singly occupied molecular orbitals (SOMOs), $5a_1$ and $4b_2$, give rise to band C, which has relatively low intensity. Electron detachment from $3b_2$ α - and β -MOs derived from the B-B σ_{2s}^* antibonding orbital (Fig. 4) account tentatively for the signals near 3.9 eV of band D. When an electron is detached from a doubly occupied MOs (α - and β -MOs with little spin polarization), it can result in either a doublet or quartet final state. Since the quartet state has a higher exchange energy, its VDE is usually lower than its doublet counterpart, as one can see in bands B and D. It should also be noted that, as is common in strongly correlated f -systems,^{89,90} generalized Koopmans' theorem (GKT) is violated even qualitatively, making it difficult

to assign PES transitions based on GKT with simple Kohn-Sham (K-S) MO energies without calculating the actual initial and final state energies of the electron detachment process. Overall, considering the complicated electron correlation and limited basis sets, the calculated VDEs from $\Delta\text{SCF-TDDFT}$ approach agree well with the experimental data, confirming the C_{2v} global minimum structure and the ground state of PrB_2^- .

3.4. The electronic structure and chemical bonding of PrB_2^-

Systematic theoretical analyses have been performed to gain insights into the electronic structure and chemical bonding of PrB_2^- . Fig. 3 depicts the radial distribution probability $D(r) = r^2 R(r)^2$ of the Pr^{3+} $5d$ and $4f$ orbitals as well as the B $2s$ and $2p$ orbitals lying at 2.3 Å (the average Pr-B distance in PrB_2^- and PrB_2). The Pr $4f$ is much more contracted ($r_{\text{max}} \sim 0.34$ Å) than the $5d$ orbitals ($r_{\text{max}} \sim 1.03$ Å) in the radial distribution, leading to nearly negligible orbital overlap between Pr $4f$ and B $2s/2p$. In contrast, the Pr $5d$ orbitals have significant orbital overlap with B $2s/2p$, which accounts for the covalent bonding interaction between Pr $5d$ and B $2s-2p$ hybrid orbitals. It is worth noting that B $2p$ orbitals are radially quite contracted because of the quantum primogenetic effect.⁹¹ As a result, both the $2p$ and $2s$ orbitals of B atom can overlap with Pr $5d$ orbitals.

Fig. 4 presents the schematic energy-level correlation diagram between the presumed fragments Pr and B_2^- . From group theory, with molecular plane σ_{yz} of C_{2v} symmetry, the Pr AOs transform as $6s$ (a_1) as well as $5d_{z^2}$ (a_1), $5d_{xz}$ (b_1), $5d_{yz}$ (b_2), $5d_{xy}$ (a_2) and $5d_{x^2-y^2}$ (a_1), respectively. As shown in Fig. 3, the Pr $4f$ orbitals are too contracted to overlap with B_2 ligand orbitals, so they span a narrow band consisting of $4f_{z^3}$ (a_1), $4f_{xz^2}$ (b_1), $4f_{yz^2}$ (b_2), $4f_{xy^2}$ (a_2), $4f_{x^2-y^2}$ (a_1), $4f_{x(x^2-y^2)}$ (b_1), $4f_{y(x^2-y^2)}$ (b_2), with the $5a_1$ and $4b_2$ α -MOs occupied in the f^2 electron configuration. As the B($2s^2 2p^1$) atom has three valence electrons, from the well-known Mulliken qualitative MO levels of diatomic molecule (Fig. 4), one can obtain the familiar



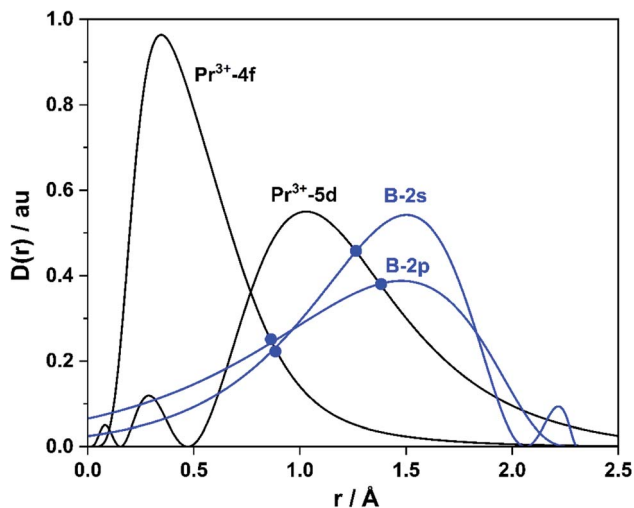


Fig. 3 Atomic valence-orbital radial-densities $D(r) = r^2 R(r)^2$ of 4f/5d orbitals (black lines) of Pr^{3+} ion with $4f^2$ configuration and of 2s/2p orbitals (blue lines) of B atom lying at 2.3 Å (from PBE density functional calculations).

$(\sigma_{2s})^2(\sigma_{2s}^*)^2(\pi_{2p})^2(\sigma_{2p})^1(\pi_{2p}^*)^0(\sigma_{2p}^*)^0$ electron configuration for B_2^- ion, where 2s/2p indicating the composing atomic orbitals (AOs) and asterisk (*) denotes antibonding MOs.

In Fig. 4, σ_{2s} of B_2^- is rather low in energy compared with the valence AOs of Pr; therefore, it participates weakly in bonding

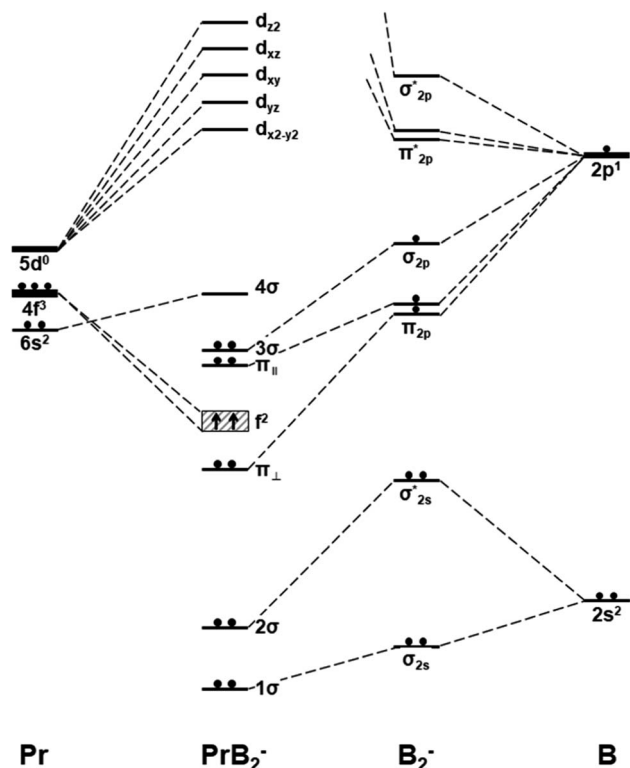
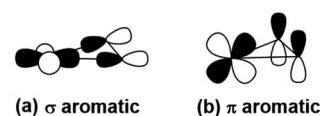


Fig. 4 Schematic orbital energy levels of triangle $\text{Pr}(\eta_2\text{-B})_2^-$, B_2^- , and Pr. The symbol $\pi_{||}$ and π_{\perp} denotes the in-plane and out-of-plane π MOs, and their respective orbital interaction with Pr $5d_{x^2-y^2}$ and $5d_{xz}$ orbitals are shown in Scheme 1.

with 6s as well as $5d_{z^2}/5d_{x^2-y^2}$ when Pr is coordinated by B_2^- . However, as the size of B 2s is as large as the 2p orbitals based on the radial distribution function (Fig. 3), B 2s can interact with Pr 5d orbitals when they are not too far apart energetically. Indeed, the antibonding σ_{2s}^* MO in B_2^- forms the bonding $3b_2$ MO upon interaction with Pr $5d_{yz}$ AOs. The two degenerate π_{2p} MOs of B_2^- also interact with the Pr 5d AOs, in two different ways: the π_{2p} MO perpendicular to the molecular plane (π_{\perp}) forms a $3c-2e$ π bonding $2b_1$ MO with Pr $5d_{xz}$ while the π_{2p} MO in the plane of the molecule ($\pi_{||}$) forms a $3c-2e$ σ bonding $6a_1$ MO with Pr $5d_{z^2}/5d_{x^2-y^2}$ AOs, as is illustrated in Scheme 1. The σ_{2p} MO of B_2^- is slightly stabilized by interacting with Pr 6s as well as $5d_{z^2}/5d_{x^2-y^2}$ AOs. As a result, the Pr 6s AO has been pushed up significantly by interacting with the σ_{2s} and σ_{2p} MOs of B_2^- with the same symmetry, forming the lowest unoccupied MO (4σ). Overall, the orbital interaction between σ_{2p} and π_{2p} MOs of B_2^- and Pr 5d/6s AOs leads to significant bonding stabilization of π_{\perp} , $\pi_{||}$, and 3σ MOs of PrB_2^- , which causes Pr to lose three electrons to fill the B-2p based MOs to form the electron configuration of $(\pi_{\perp})^2(\pi_{||})^2(\sigma_{BB})^2 \text{Pr}^{\text{III}}(4f^2 6s^0)$. Therefore, the PrB_2^- molecule can be described as composed of a +3-oxidation-state Pr^{3+} (*i.e.*, Pr^{III}) with f^2 -configuration and formally a coordinated B_2^{4-} tetraanion, namely $\text{Pr}^{\text{III}}[\text{B}_2^{4-}]$. Interestingly, the B_2^{4-} tetraanion is isoelectronic with the C_2^{2-} , N_2 , and O_2^{2+} diatomic moiety that has the well-known $(\sigma_{2s})^2(\sigma_{2s}^*)^2(\pi_{2p})^4(\sigma_{2p})^2(\pi_{2p}^*)^0(\sigma_{2p}^*)^0$ electron configuration, despite the much higher σ_{2p} and π_{2p} orbital energies of B_2^{4-} due to smaller electronegativity of B than C, N and O. The spin-polarized α and β sets of MOs and the contour surfaces of the PrB_2^- valence MOs are shown in Table 2. Therefore, there are five sets of interactions among the three atoms of PrB_2^- , including the $\alpha + \beta$ sets of $4a_1$, $3b_2$, $2b_1$, as well as the more spin polarized $6a_1\alpha + 6a_1\beta$ and $7a_1\alpha + 5a_1\beta$.

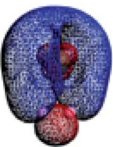
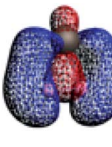
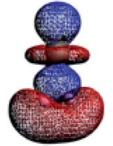
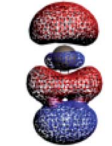
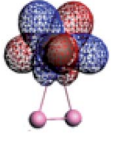
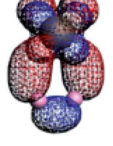



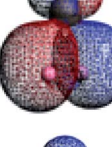
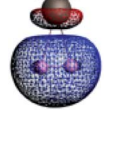

It should be noted that the nearly degenerate 4f MO levels are stabilized in $\text{Pr}(\text{III})$ and slightly split due to the presence of B_2^- , similar to the crystal field splitting. As a result, the lowest energy state corresponds to the two 4f electrons staying in two specific 4f MOs, *i.e.*, the $5a_1\alpha$ and $4b_2\alpha$ sets, forming a paramagnetic ground state. The calculated magnetic exchange coupling constant $J = -\frac{E_{\text{HS}} - E_{\text{BS}}}{\langle \hat{S}^2 \rangle_{\text{HS}} - \langle \hat{S}^2 \rangle_{\text{BS}}} = 6703 \text{ cm}^{-1}$, where E_{HS} and E_{BS} are the energies of the triplet high-spin (HS) and broken-symmetry (BS) singlet states. However, in DFT calculations, due to the self-interaction error (SIE)⁹² and hybrid mixing of Hartree-Fock exchange, virtual 4f orbitals are much higher in energy, resulting in only two occupied 4f α -MOs having relatively low energies.



Scheme 1 The σ -type and π -type orbital interaction between Pr-5d and B-2p orbitals, leading to (a) σ - and (b) π -metalla-aromaticity, respectively.



Table 2 The spin-polarized α and β set Kohn–Sham MOs of PrB_2^- calculated at the PBE0/TZP level using ADF code. Colour codes: olive – Pr; pink – B

α – MO					β – MO				
Kind	Irrep.	$-\varepsilon_i$ (eV)	MO% (Pr : B ₂)	Contour	Kind	Irrep.	$-\varepsilon_i$ (eV)	MO% (Pr : B ₂)	Contour
3 σ	7a ₁	1.78	70 : 30		3 σ	5a ₁	1.97	44 : 56	
π_{\parallel}	6a ₁	1.90	37 : 63		π_{\parallel}	6a ₁	1.77	40 : 60	
f ²	4b ₂	2.26	97 : 3						
f ²	5a ₁	2.33	91 : 9						
π_{\perp}	2b ₁	2.46	38 : 62		π_{\perp}	2b ₁	2.43	33 : 67	
2 σ	3b ₂	3.95	36 : 64		2 σ	3b ₂	4.00	26 : 74	
1 σ	4a ₁	9.26	16 : 84		1 σ	4a ₁	9.35	15 : 85	

Interestingly, the linear Pr–B–B isomer shares a similar bonding pattern with the C_{2v} global minimum (Fig. S4–S5 and Table S7†). The σ_{2s} MO is still too low in energy to be bonded with Pr, and the bonding 6 σ MO is formed by σ_{2s}^* . The two π_{2p} MOs in B_2^- form a pair of degenerate π bonding MOs with Pr 5d AOs. Also, the 6s AO in Pr is now non-bonded and occupied in the 7 $\sigma\alpha$ MO, while σ_{2p} interacts with a 5d AO forming a 7 $\sigma\beta$ bonding MO. The Pr oxidation state of this linear isomer is thus +2. As the 6s electron is unpaired, the total bonding interaction in the linear structure is weaker than that in the triangle structure, implying that a linear PrB_2^- would tend to bend into a triangle arrangement by the second-order Jahn–Teller effect.⁹³

The global minimum of PrB_2^- is found to be doubly aromatic, as verified by various analyses including the canonical K–S MOs, adaptive natural density partitioning⁸¹ (AdNDP) analysis, induced ring-current strength,⁷⁶ the anisotropy of the induced current density⁷⁵ (AICD), the diamagnetic anisotropy,⁷² the nucleus-independent chemical shift (NICS)⁷³ and the bifurcation analysis of electron localization function (ELF) of the σ and π electrons.⁹⁴ In the K–S MOs, there are two delocalized 3c–2e MOs consisting of Pr and B₂ moiety: a σ bonding MO of 6a₁ and a π bonding MO of 2b₁. These two delocalized 3c–2e bonding MOs of 6a₁ and 2b₁ in Table 2 can also be verified by the AdNDP results (Fig. 5), where the first row describes three localized σ bonds and the



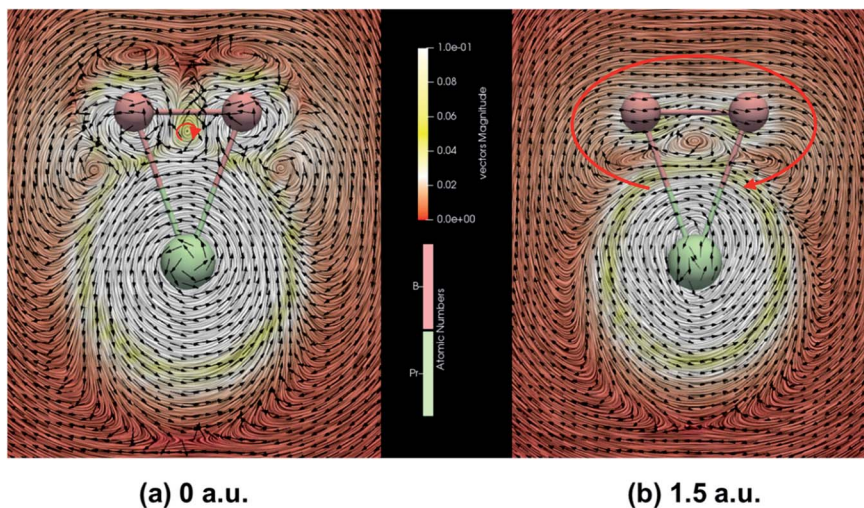


Fig. 6 The strength and direction of the induced current of PrB_2^- at (a) the molecular plane and (b) 1.5 a.u. above the molecular plane calculated by the GIMIC program with MWB28 ECP and basis set for Pr and cc-pVTZ basis set for B. The magnetic field is pointing out of the molecule plane. Black arrows indicate the direction of the current. Clockwise currents represented by red arrows are diatropic and indicate aromaticity.

have a 5/3 bond order by Kuznetsov and Boldyrev.¹⁰⁷ Finally, the five types of bond order indices^{83–86} listed in Table 4 reveal that both Pr–B interactions in PrB_2^- have a bond order greater than one, consistent with the Pr–B multiple bond character. Interestingly, both the Gopinathan–Jug bond order and the Nalewajski–Mrozek bond orders support the assignment of triple $\text{B}\equiv\text{B}$ bond in the B_2^{4-} tetraanion, similar to the isoelectronic $\text{N}\equiv\text{N}$.

4 Conclusion

In summary, we report a photoelectron spectroscopy and quantum chemistry study of PrB_2^- , which is found to have a C_{2v} unilateral triangle structure with a paramagnetic triplet ground state $^3\text{B}_2$. The Pr atom is shown to lose three electrons to form the trivalent Pr(III) with f^2 configuration and an unprecedented B_2^{4-} tetraanion, which is in contrast to the PrB_x^- ($x = 3, 4$) clusters with Pr(II) and B_3^{3-} as well as Pr(I) and B_4^{2-} , respectively.¹⁰⁸ The π orbitals of the $\text{B}\equiv\text{B}$ triple bonds in B_2^{4-} participate in bonding with Pr^{III} , forming an in-plane σ -type and out-of-plane π -type three-centred delocalized systems (Scheme 1) and giving rise to double aromaticity involving a 4f metal atom. The localized peripheral Pr–B σ -bond plus the two 3c–2e delocalized bonds results in multiple bond characters for the Pr–B bonds. The current study demonstrates that metallaromaticity and multiple chemical bonds between 4f metals and boron are viable and broadens the chemistry between lanthanide and boron. The present work also reveals that the high-lying 5d orbitals of the 4f-elements can facilitate the formation of the B_2^{4-} tetraanion, which complete the isoelectronic B_2^{4-} , C_2^{2-} and N_2 and O_2^{2+} series.^{109,110} The insight of the characteristic high-lying 5d orbitals of the 4f-elements can provide guidance in preparing organometallic complexes with highly negatively charged organic ligands of rare-earth elements.^{111,112}

Data availability

The data that supports the findings of this study is available from the corresponding author upon reasonable request.

Author contributions

H. S. H. and L. S. W. designed the project. T. T. C. and W. J. C. performed the experiments. Z. L. W., W. L. L., J. Z., and X. L. J. performed the computational calculations. Z. L. W., T. T. C., J. L., L. S. W. and H. S. H. wrote and edited the manuscript. All authors helped to analyse the experimental and theoretical results.

Conflicts of interest

The authors declare no conflict of interest.

Acknowledgements

The experiment done at Brown University was supported by the National Science Foundation (CHE-2053541). The theoretical work was supported by the National Natural Science Foundation of China (Grant No. 21906094, 22076095, 22033005) and the support of Guangdong Provincial Key Laboratory of Catalysis (No. 2020B121201002). The calculations were done using supercomputers at Tsinghua National Laboratory for Information Science and Technology, and the Computational Chemistry Laboratory of the Department of Chemistry under the Tsinghua Xuetang Talents Program.

References

- J. Chandrasekhar, E. D. Jemmis and P. von Ragué Schleyer, Double Aromaticity: Aromaticity in Orthogonal Planes. The



- 3,5-Dehydrophenyl Cation, *Tetrahedron Lett.*, 1979, **20**(39), 3707–3710, DOI: [10.1016/S0040-4039\(01\)95503-0](https://doi.org/10.1016/S0040-4039(01)95503-0).
- 2 D. L. Thorn and R. Hoffman, Delocalization in Metallacycles, *Nouv. J. Chim.*, 1979, **3**, 39–45.
- 3 D. Chen, Y. Hua and H. Xia, Metallaaromatic Chemistry: History and Development, *Chem. Rev.*, 2020, **120**(23), 12994–13086, DOI: [10.1021/acs.chemrev.0c00392](https://doi.org/10.1021/acs.chemrev.0c00392).
- 4 I. Fernández, G. Frenking and G. Merino, Aromaticity of Metallabenzenes and Related Compounds, *Chem. Soc. Rev.*, 2015, **44**(18), 6452–6463, DOI: [10.1039/c5cs00004a](https://doi.org/10.1039/c5cs00004a).
- 5 A. I. Boldyrev and L. S. Wang, All-Metal Aromaticity and Antiaromaticity, *Chem. Rev.*, 2005, **105**(10), 3716–3757, DOI: [10.1021/cr030091t](https://doi.org/10.1021/cr030091t).
- 6 D. Y. Zubarev, B. B. Averkiev, H. J. Zhai, L. S. Wang and A. I. Boldyrev, Aromaticity and Antiaromaticity in Transition-Metal Systems, *Phys. Chem. Chem. Phys.*, 2008, **10**(2), 257–267, DOI: [10.1039/b713646c](https://doi.org/10.1039/b713646c).
- 7 B. B. Averkiev and A. I. Boldyrev, Hf₃ Cluster Is Triply (σ -, π -, and δ -) Aromatic in the Lowest D_{3h}, ¹A₁' State, *J. Phys. Chem. A*, 2007, **111**(50), 12864–12866, DOI: [10.1021/jp077528b](https://doi.org/10.1021/jp077528b).
- 8 A. C. Tsepis, C. E. Kefalidis and C. A. Tsepis, The Role of the 5f Orbitals in Bonding, Aromaticity, and Reactivity of Planar Isocyclic and Heterocyclic Uranium Clusters, *J. Am. Chem. Soc.*, 2008, **130**(28), 9144–9155, DOI: [10.1021/ja802344z](https://doi.org/10.1021/ja802344z).
- 9 D. Y. Zubarev and A. I. Boldyrev, Multiple Aromaticity, Multiple Antiaromaticity, and Conflicting Aromaticity in Inorganic Systems, *Encycl. Inorg. Chem.*, 2009, DOI: [10.1002/0470862106.ia633](https://doi.org/10.1002/0470862106.ia633).
- 10 C. A. Tsepis, Aromaticity/Antiaromaticity in “Bare” and “Ligand-Stabilized” Rings of Metal Atoms, *Structure and Bonding*, ed. Parkin G., Springer Berlin Heidelberg, Berlin, Heidelberg, 2010, vol. 136, pp. 217–274. DOI: [10.1007/978-3-642-05243-9_7](https://doi.org/10.1007/978-3-642-05243-9_7).
- 11 A. P. Sergeeva, B. B. Averkiev, and A. I. Boldyrev, All-Transition Metal Aromaticity and Antiaromaticity, ed. Parkin G., *Structure and Bonding*, Springer Berlin Heidelberg, Berlin, Heidelberg, 2010, vol. 136, pp. 275–305. DOI: [10.1007/978-3-642-05243-9_8](https://doi.org/10.1007/978-3-642-05243-9_8).
- 12 J. Li, C.-W. Liu and J.-X. Lu, Ab Initio Studies of Electronic Structures and Quasi-Aromaticity in M₃S_{4-n}O⁴⁺_n (M = Mo, W; n = 0–4) Clusters, *J. Chem. Soc., Faraday Trans.*, 1994, **90**(1), 39–45, DOI: [10.1039/FT9949000039](https://doi.org/10.1039/FT9949000039).
- 13 X. Li, A. E. Kuznetsov, H.-F. Zhang, A. I. Boldyrev and L.-S. Wang, Observation of All-Metal Aromatic Molecules, *Science*, 2001, **291**(5505), 859–861, DOI: [10.1126/science.291.5505.859](https://doi.org/10.1126/science.291.5505.859).
- 14 A. N. Alexandrova and A. I. Boldyrev, σ -Aromaticity and σ -Antiaromaticity in Alkali Metal and Alkaline Earth Metal Small Clusters, *J. Phys. Chem. A*, 2003, **107**(4), 554–560, DOI: [10.1021/jp027008a](https://doi.org/10.1021/jp027008a).
- 15 A. E. Kuznetsov, J. D. Corbett, L.-S. Wang and A. I. Boldyrev, Aromatic Mercury Clusters in Ancient Amalgams, *Angew. Chem., Int. Ed.*, 2001, **40**(18), 3369–3372, DOI: [10.1002/1521-3773\(20010917\)40:18<3369::AID-ANIE3369>3.0.CO;2-Z](https://doi.org/10.1002/1521-3773(20010917)40:18<3369::AID-ANIE3369>3.0.CO;2-Z).
- 16 H.-J. Zhai, B. B. Averkiev, D. Y. Zubarev, L. Wang and A. I. Boldyrev, δ Aromaticity in [Ta₃O₃]⁻, *Angew. Chem., Int. Ed.*, 2007, **46**(23), 4277–4280, DOI: [10.1002/anie.200700442](https://doi.org/10.1002/anie.200700442).
- 17 M. Zhou, N. Tsumori, Z. Li, K. Fan, L. Andrews and Q. Xu, OCBBCO: A Neutral Molecule with Some Boron-Boron Triple Bond Character, *J. Am. Chem. Soc.*, 2002, **124**(44), 12936–12937, DOI: [10.1021/ja026257+](https://doi.org/10.1021/ja026257+).
- 18 W.-L. Li, H.-S. Hu, Y.-F. Zhao, X. Chen, T.-T. Chen, T. Jian, L.-S. Wang and J. Li, Recent Progress on the Investigations of Boron Clusters and Boron-Based Materials (I): Borophene, *Sci. Sin.: Chim.*, 2018, **48**(2), 98–107, DOI: [10.1360/N032017-00185](https://doi.org/10.1360/N032017-00185).
- 19 T. Mori, Lanthanides: Boride, Carbide, and Nitride Compounds, in *Encyclopedia of Inorganic and Bioinorganic Chemistry*, John Wiley & Sons, Ltd, Chichester, UK, 2012. DOI: [10.1002/9781119951438.eibc2028](https://doi.org/10.1002/9781119951438.eibc2028).
- 20 T. Jian, X. Chen, S. D. Li, A. I. Boldyrev, J. Li and L. S. Wang, Probing the Structures and Bonding of Size-Selected Boron and Doped-Boron Clusters, *Chem. Soc. Rev.*, 2019, **48**(13), 3550–3591, DOI: [10.1039/c9cs00233b](https://doi.org/10.1039/c9cs00233b).
- 21 A. P. Sergeeva, I. A. Popov, Z. A. Piazza, W.-L. Li, C. Romanescu, L.-S. Wang and A. I. Boldyrev, Understanding Boron through Size-Selected Clusters: Structure, Chemical Bonding, and Fluxionality, *Acc. Chem. Res.*, 2014, **47**(4), 1349–1358, DOI: [10.1021/ar400310g](https://doi.org/10.1021/ar400310g).
- 22 H. J. Zhai, A. N. Alexandrova, K. A. Birch, A. I. Boldyrev and L. S. Wang, Hepta- and Octacoordinate Boron in Molecular Wheels of Eight- and Nine-Atom Boron Clusters: Observation and Confirmation, *Angew. Chem., Int. Ed.*, 2003, **42**(48), 6004–6008, DOI: [10.1002/anie.200351874](https://doi.org/10.1002/anie.200351874).
- 23 H. J. Zhai, B. Kiran, J. Li and L. S. Wang, Hydrocarbon Analogues of Boron Clusters Planarity, Aromaticity and Antiaromaticity, *Nat. Mater.*, 2003, **2**(12), 827–833, DOI: [10.1038/nmat1012](https://doi.org/10.1038/nmat1012).
- 24 D. Y. Zubarev and A. I. Boldyrev, Comprehensive Analysis of Chemical Bonding in Boron Clusters, *J. Comput. Chem.*, 2007, **28**(1), 251–268, DOI: [10.1002/jcc.20518](https://doi.org/10.1002/jcc.20518).
- 25 A. I. Boldyrev and L.-S. Wang, Beyond Organic Chemistry: Aromaticity in Atomic Clusters, *Phys. Chem. Chem. Phys.*, 2016, **18**(17), 11589–11605, DOI: [10.1039/C5CP07465G](https://doi.org/10.1039/C5CP07465G).
- 26 W. Li, T. Jian, X. Chen, T. Chen, G. V. Lopez, J. Li and L. Wang, The Planar CoB₁₈⁻ Cluster as a Motif for Metallo-Borophenes, *Angew. Chem., Int. Ed.*, 2016, **55**(26), 7358–7363, DOI: [10.1002/anie.201601548](https://doi.org/10.1002/anie.201601548).
- 27 T. Jian, W.-L. Li, X. Chen, T.-T. Chen, G. V. Lopez, J. Li and L.-S. Wang, Competition between Drum and Quasi-Planar Structures in RhB₁₈⁻: Motifs for Metallo-Boronanotubes and Metallo-Borophenes, *Chem. Sci.*, 2016, **7**(12), 7020–7027, DOI: [10.1039/C6SC02623K](https://doi.org/10.1039/C6SC02623K).
- 28 W.-L. Li, X. Chen, T. Jian, T.-T. Chen, J. Li and L.-S. Wang, From Planar Boron Clusters to Borophenes and Metalloborophenes, *Nat. Rev. Chem.*, 2017, **1**(10), 0071, DOI: [10.1038/s41570-017-0071](https://doi.org/10.1038/s41570-017-0071).
- 29 C. Romanescu, T. R. Galeev, W.-L. Li, A. I. Boldyrev and L.-S. Wang, Aromatic Metal-Centered Monocyclic Boron Rings: Co@B₈⁻ and Ru@B₉⁻, *Angew. Chem., Int. Ed.*, 2011, **50**(40), 9334–9337, DOI: [10.1002/anie.201104166](https://doi.org/10.1002/anie.201104166).



- 30 T. R. Galeev, C. Romanescu, W.-L. Li, L.-S. Wang and A. I. Boldyrev, Observation of the Highest Coordination Number in Planar Species: Decacoordinated $\text{Ta}@\text{B}_{10}^-$ and $\text{Nb}@\text{B}_{10}^-$ Anions, *Angew. Chem., Int. Ed.*, 2012, **51**(9), 2101–2105, DOI: [10.1002/anie.201107880](https://doi.org/10.1002/anie.201107880).
- 31 W.-L. Li, C. Romanescu, T. R. Galeev, Z. A. Piazza, A. I. Boldyrev and L.-S. Wang, Transition-Metal-Centered Nine-Membered Boron Rings: $\text{M}@\text{B}_9$ and $\text{M}@\text{B}_9^-$ ($\text{M} = \text{Rh}, \text{Ir}$), *J. Am. Chem. Soc.*, 2012, **134**(1), 165–168, DOI: [10.1021/ja209808k](https://doi.org/10.1021/ja209808k).
- 32 C. Romanescu, T. R. Galeev, A. P. Sergeeva, W.-L. Li, L.-S. Wang and A. I. Boldyrev, Experimental and Computational Evidence of Octa- and Nona-Coordinated Planar Iron-Doped Boron Clusters: $\text{Fe}@\text{B}_8^-$ and $\text{Fe}@\text{B}_9^-$, *J. Organomet. Chem.*, 2012, **721–722**, 148–154, DOI: [10.1016/j.jorganchem.2012.07.050](https://doi.org/10.1016/j.jorganchem.2012.07.050).
- 33 C. Romanescu, T. R. Galeev, W.-L. Li, A. I. Boldyrev and L.-S. Wang, Transition-Metal-Centered Monocyclic Boron Wheel Clusters ($\text{M}@\text{B}_n$): A New Class of Aromatic Borometallic Compounds, *Acc. Chem. Res.*, 2013, **46**(2), 350–358, DOI: [10.1021/ar300149a](https://doi.org/10.1021/ar300149a).
- 34 T.-T. Chen, W.-L. Li, H. Bai, W.-J. Chen, X.-R. Dong, J. Li and L.-S. Wang, $\text{Re}@\text{B}_8^-$ and $\text{Re}@\text{B}_9^-$: New Members of the Transition-Metal-Centered Borometallic Molecular Wheel Family, *J. Phys. Chem. A*, 2019, **123**(25), 5317–5324, DOI: [10.1021/acs.jpca.9b03942](https://doi.org/10.1021/acs.jpca.9b03942).
- 35 L. F. Cheung, G. S. Kocheril, J. Czekner and L.-S. Wang, Observation of Möbius Aromatic Planar Metallaborocycles, *J. Am. Chem. Soc.*, 2020, **142**(7), 3356–3360, DOI: [10.1021/jacs.9b13417](https://doi.org/10.1021/jacs.9b13417).
- 36 L. F. Cheung, J. Czekner, G. S. Kocheril and L. S. Wang, ReB_6^- : A Metallaboron Analog of Metallabenzenes, *J. Am. Chem. Soc.*, 2019, **141**(44), 17854–17860, DOI: [10.1021/jacs.9b09110](https://doi.org/10.1021/jacs.9b09110).
- 37 Y. Tang, S. Zhao, B. Long, J.-C. Liu and J. Li, On the Nature of Support Effects of Metal Dioxides MO_2 ($\text{M} = \text{Ti}, \text{Zr}, \text{Hf}, \text{Ce}, \text{Th}$) in Single-Atom Gold Catalysts: Importance of Quantum Primogenic Effect, *J. Phys. Chem. C*, 2016, **120**(31), 17514–17526, DOI: [10.1021/acs.jpcc.6b05338](https://doi.org/10.1021/acs.jpcc.6b05338).
- 38 J.-B. Lu, D. C. Cantu, M.-T. Nguyen, J. Li, V.-A. Glezakou and R. Rousseau, Norm-Conserving Pseudopotentials and Basis Sets To Explore Lanthanide Chemistry in Complex Environments, *J. Chem. Theory Comput.*, 2019, **15**(11), 5987–5997, DOI: [10.1021/acs.jctc.9b00553](https://doi.org/10.1021/acs.jctc.9b00553).
- 39 Y. Luo and Z. Hou, Prediction of Binary Lanthanide(III) Hydride Clusters Ln_nH_{3n} ($\text{Ln} = \text{La}, \text{Gd}, \text{and Lu}; n = 3 \text{ and } 4$), *J. Phys. Chem. C*, 2008, **112**(2), 635–638, DOI: [10.1021/jp077318z](https://doi.org/10.1021/jp077318z).
- 40 S.-B. Cheng, C. Berkdemir and A. W. Castleman, Observation of d-p Hybridized Aromaticity in Lanthanum-Doped Boron Clusters, *Phys. Chem. Chem. Phys.*, 2014, **16**(2), 533–539, DOI: [10.1039/C3CP53245C](https://doi.org/10.1039/C3CP53245C).
- 41 J. T. Boronski, J. A. Seed, D. Hunger, A. W. Woodward, J. van Slageren, A. J. Wooles, L. S. Natrajan, N. Kaltsoyannis and S. T. Liddle, A Crystalline Tri-Thorium Cluster with σ -Aromatic Metal–Metal Bonding, *Nature*, 2021, **598**(7879), 72–75, DOI: [10.1038/s41586-021-03888-3](https://doi.org/10.1038/s41586-021-03888-3).
- 42 X. X. Chi and Y. Liu, Theoretical Evidence of d-Orbital Aromaticity in Anionic Metal X_3^- ($\text{X} = \text{Sc}, \text{Y}, \text{La}$) Clusters, *Int. J. Quantum Chem.*, 2007, **107**(9), 1886–1896, DOI: [10.1002/qua.21326](https://doi.org/10.1002/qua.21326).
- 43 A. S. Ivanov, X. Zhang, H. Wang, A. I. Boldyrev, G. Gantefoer, K. H. Bowen and I. Černušák, Anion Photoelectron Spectroscopy and CASSCF/CASPT2/RASSI Study of La_n^- ($n = 1, 3–7$), *J. Phys. Chem. A*, 2015, **119**(46), 11293–11303, DOI: [10.1021/acs.jpca.5b08076](https://doi.org/10.1021/acs.jpca.5b08076).
- 44 O. T. Summerscales and J. C. Gordon, Complexes Containing Multiple Bonding Interactions between Lanthanoid Elements and Main-Group Fragments, *RSC Adv.*, 2013, **3**(19), 6682–6692, DOI: [10.1039/c3ra23151h](https://doi.org/10.1039/c3ra23151h).
- 45 Q. Zhu, J. Zhu and C. Zhu, Recent Progress in the Chemistry of Lanthanide-Ligand Multiple Bonds, *Tetrahedron Lett.*, 2018, **59**(6), 514–520, DOI: [10.1016/j.tetlet.2017.12.079](https://doi.org/10.1016/j.tetlet.2017.12.079).
- 46 D. Schädle and R. Anwander, Rare-Earth Metal and Actinide Organoimide Chemistry, *Chem. Soc. Rev.*, 2019, **48**(24), 5752–5805, DOI: [10.1039/c8cs00932e](https://doi.org/10.1039/c8cs00932e).
- 47 T. Cheisson, K. D. Kersey, N. Mahieu, A. McSkimming, M. R. Gau, P. J. Carroll and E. J. Schelter, Multiple Bonding in Lanthanides and Actinides: Direct Comparison of Covalency in Thorium(IV)- and Cerium(IV)-Imido Complexes, *J. Am. Chem. Soc.*, 2019, **141**(23), 9185–9190, DOI: [10.1021/jacs.9b04061](https://doi.org/10.1021/jacs.9b04061).
- 48 T. T. Chen, W. L. Li, T. Jian, X. Chen, J. Li and L. S. Wang, PrB_7^- : A Praseodymium-Doped Boron Cluster with a Pr^{II} Center Coordinated by a Doubly Aromatic Planar $\eta^7\text{-B}_7^{3-}$ Ligand, *Angew. Chem., Int. Ed.*, 2017, **56**(24), 6916–6920, DOI: [10.1002/anie.201703111](https://doi.org/10.1002/anie.201703111).
- 49 W. L. Li, T. T. Chen, D. H. Xing, X. Chen, J. Li and L. S. Wang, Observation of Highly Stable and Symmetric Lanthanide Octa-Boron Inverse Sandwich Complexes, *Proc. Natl. Acad. Sci. U. S. A.*, 2018, **115**(30), E6972–E6977, DOI: [10.1073/pnas.1806476115](https://doi.org/10.1073/pnas.1806476115).
- 50 T. T. Chen, W. L. Li, J. Li and L. S. Wang, $[\text{La}(\text{H}_x\text{-B}_x)\text{La}]^-$ ($x = 7–9$): A New Class of Inverse Sandwich Complexes, *Chem. Sci.*, 2019, **10**(8), 2534–2542, DOI: [10.1039/c8sc05443f](https://doi.org/10.1039/c8sc05443f).
- 51 Z.-Y. Jiang, T.-T. Chen, W.-J. Chen, W.-L. Li, J. Li and L.-S. Wang, Expanded Inverse-Sandwich Complexes of Lanthanum Borides: $\text{La}_2\text{B}_{10}^-$ and $\text{La}_2\text{B}_{11}^-$, *J. Phys. Chem. A*, 2021, **125**(12), 2622–2630, DOI: [10.1021/acs.jpca.1c01149](https://doi.org/10.1021/acs.jpca.1c01149).
- 52 T. T. Chen, W. L. Li, W. J. Chen, J. Li and L. S. Wang, $\text{La}_3\text{B}_{14}^-$: An Inverse Triple-Decker Lanthanide Boron Cluster, *Chem. Commun.*, 2019, **55**(54), 7864–7867, DOI: [10.1039/c9cc03807h](https://doi.org/10.1039/c9cc03807h).
- 53 T.-T. Chen, W.-L. Li, W.-J. Chen, X.-H. Yu, X.-R. Dong, J. Li and L.-S. Wang, Spherical Trihedral Metallo-Borosphenes, *Nat. Commun.*, 2020, **11**(1), 2766, DOI: [10.1038/s41467-020-16532-x](https://doi.org/10.1038/s41467-020-16532-x).
- 54 L. S. Wang, H. S. Cheng and J. Fan, Photoelectron Spectroscopy of Size-Selected Transition Metal Clusters: Fe_n^- , $n = 3–24$, *J. Chem. Phys.*, 1995, **102**(24), 9480–9493, DOI: [10.1063/1.468817](https://doi.org/10.1063/1.468817).
- 55 L. S. Wang, Photoelectron Spectroscopy of Size-Selected Boron Clusters: From Planar Structures to Borophenes



- 80 J. X. Zhang, F. K. Sheong and Z. Lin, Unravelling Chemical Interactions with Principal Interacting Orbital Analysis, *Chem.–A Eur. J.*, 2018, **24**(38), 9639–9650, DOI: [10.1002/chem.201801220](https://doi.org/10.1002/chem.201801220).
- 81 D. Y. Zubarev and A. I. Boldyrev, Developing Paradigms of Chemical Bonding: Adaptive Natural Density Partitioning, *Phys. Chem. Chem. Phys.*, 2008, **10**(34), 5207–5217, DOI: [10.1039/b804083d](https://doi.org/10.1039/b804083d).
- 82 T. Lu and F. M. Chen, A Multifunctional Wavefunction Analyzer, *J. Comput. Chem.*, 2012, **33**(5), 580–592, DOI: [10.1002/jcc.22885](https://doi.org/10.1002/jcc.22885).
- 83 I. Mayer, Bond Order and Valence Indices: A Personal Account, *J. Comput. Chem.*, 2007, **28**(1), 204–221, DOI: [10.1002/jcc.20494](https://doi.org/10.1002/jcc.20494).
- 84 M. S. Gopinathan and K. Jug, Valency. I. A Quantum Chemical Definition and Properties, *Theor. Chim. Acta*, 1983, **63**(6), 497–509, DOI: [10.1007/BF02394809](https://doi.org/10.1007/BF02394809).
- 85 A. Michalak, R. L. Dekock and T. Ziegler, Bond Multiplicity in Transition-Metal Complexes: Applications of Two-Electron Valence Indices, *J. Phys. Chem. A*, 2008, **112**(31), 7256–7263, DOI: [10.1021/jp800139g](https://doi.org/10.1021/jp800139g).
- 86 R. F. Nalewajski, J. Mrozek and A. Michalak, Two-Electron Valence Indices from the Kohn-Sham Orbitals, *Int. J. Quantum Chem.*, 1997, **61**(3), 589–601, DOI: [10.1002/\(SICI\)1097-461X\(1997\)61:3<589::AID-QUA28>3.0.CO;2-2](https://doi.org/10.1002/(SICI)1097-461X(1997)61:3<589::AID-QUA28>3.0.CO;2-2).
- 87 R. O. Jones and O. Gunnarsson, The Density Functional Formalism, Its Applications and Prospects, *Rev. Mod. Phys.*, 1989, **61**(3), 689–746, DOI: [10.1103/RevModPhys.61.689](https://doi.org/10.1103/RevModPhys.61.689).
- 88 J. Li, X. Li, H.-J. Zhai and L.-S. Wang, Au₂₀: A Tetrahedral Cluster, *Science*, 2003, **299**(5608), 864–867, DOI: [10.1126/science.1079879](https://doi.org/10.1126/science.1079879).
- 89 W. L. Li, J. Su, T. Jian, G. V. Lopez, H. S. Hu, G. J. Cao, J. Li and L. S. Wang, Strong Electron Correlation in UO₂: A Photoelectron Spectroscopy and Relativistic Quantum Chemistry Study, *J. Chem. Phys.*, 2014, **140**(9), DOI: [10.1063/1.4867278](https://doi.org/10.1063/1.4867278).
- 90 J. Su, W. L. Li, G. V. Lopez, T. Jian, G. J. Cao, W. L. Li, W. H. E. Schwarz, L. S. Wang and J. Li, Probing the Electronic Structure and Chemical Bonding of Mono-Uranium Oxides with Different Oxidation States: UO_x[−] and UO_x (x = 3–5), *J. Phys. Chem. A*, 2016, **120**(7), 1084–1096, DOI: [10.1021/acs.jpca.5b11354](https://doi.org/10.1021/acs.jpca.5b11354).
- 91 Z. L. Wang, H. S. Hu, L. von Szentpály, H. Stoll, S. Fritzsche, P. Pykkö, W. H. E. Schwarz and J. Li, Understanding the Uniqueness of 2p Elements in Periodic Tables, *Chem.–A Eur. J.*, 2020, **26**(67), 15558–15564, DOI: [10.1002/chem.202003920](https://doi.org/10.1002/chem.202003920).
- 92 D. R. Lonsdale and L. Goerigk, The One-Electron Self-Interaction Error in 74 Density Functional Approximations: A Case Study on Hydrogenic Mono- And Dinuclear Systems, *Phys. Chem. Chem. Phys.*, 2020, **22**(28), 15805–15830, DOI: [10.1039/d0cp01275k](https://doi.org/10.1039/d0cp01275k).
- 93 R. G. Pearson, The Second-Order Jahn-Teller Effect, *J. Mol. Struct.: THEOCHEM*, 1983, **103**, 25–34, DOI: [10.1016/0166-1280\(83\)85006-4](https://doi.org/10.1016/0166-1280(83)85006-4).
- 94 J. C. Santos, W. Tiznado, R. Contreas and P. Fuentealba, Sigma-Pi Separation of the Electron Localization Function and Aromaticity, *J. Chem. Phys.*, 2004, **120**(4), 1670–1672, DOI: [10.1063/1.1635799](https://doi.org/10.1063/1.1635799).
- 95 Z.-J. Lv, Z. Huang, J. Shen, W.-X. Zhang and Z. Xi, Well-Defined Scandacyclopropenes: Synthesis, Structure, and Reactivity, *J. Am. Chem. Soc.*, 2019, **141**(51), 20547–20555, DOI: [10.1021/jacs.9b11631](https://doi.org/10.1021/jacs.9b11631).
- 96 B. J. R. Cuyacot and C. Foroutan-Nejad, $[\{\text{Th}(\text{C}_8\text{H}_8)\text{Cl}_2\}_3]^{2-}$ Is Stable but Not Aromatic, *Nature*, 2022, **603**(7902), E18–E20, DOI: [10.1038/s41586-021-04319-z](https://doi.org/10.1038/s41586-021-04319-z).
- 97 Z. Badri, S. Pathak, H. Fliegl, P. Rashidi-Ranjbar, R. Bast, R. Marek, C. Foroutan-Nejad and K. Ruud, All-Metal Aromaticity: Revisiting the Ring Current Model among Transition Metal Clusters, *J. Chem. Theory Comput.*, 2013, **9**(11), 4789–4796, DOI: [10.1021/ct4007184](https://doi.org/10.1021/ct4007184).
- 98 C. Foroutan-Nejad, J. Vicha and A. Ghosh, Relativity or Aromaticity? A First-Principles Perspective of Chemical Shifts in Osmabenzene and Osmapentalene Derivatives, *Phys. Chem. Chem. Phys.*, 2020, **22**(19), 10863–10869, DOI: [10.1039/D0CP01481H](https://doi.org/10.1039/D0CP01481H).
- 99 C. Foroutan-Nejad, Is NICS a Reliable Aromaticity Index for Transition Metal Clusters?, *Theor. Chem. Acc.*, 2015, **134**(2), 8, DOI: [10.1007/s00214-015-1617-7](https://doi.org/10.1007/s00214-015-1617-7).
- 100 M. Orozco-Ic, N. D. Charistos, A. Muñoz-Castro, R. Islas, D. Sundholm and G. Merino, Core-Electron Contributions to the Molecular Magnetic Response, *Phys. Chem. Chem. Phys.*, 2022, **24**(20), 12158–12166, DOI: [10.1039/D1CP05713H](https://doi.org/10.1039/D1CP05713H).
- 101 C. Foroutan-Nejad, S. Shahbazian and P. Rashidi-Ranjbar, The Electron Density vs. NICS Scan: A New Approach to Assess Aromaticity in Molecules with Different Ring Sizes, *Phys. Chem. Chem. Phys.*, 2010, **12**(39), 12630, DOI: [10.1039/c004254d](https://doi.org/10.1039/c004254d).
- 102 C. Foroutan-Nejad, Z. Badri, S. Shahbazian and P. Rashidi-Ranjbar, The Laplacian of Electron Density versus NICS_{zz} Scan: Measuring Magnetic Aromaticity among Molecules with Different Atom Types, *J. Phys. Chem. A*, 2011, **115**(45), 12708–12714, DOI: [10.1021/jp203681x](https://doi.org/10.1021/jp203681x).
- 103 A. C. Castro, E. Osorio, J. O. C. Jiménez-Halla, E. Matito, W. Tiznado and G. Merino, Scalar and Spin–Orbit Relativistic Corrections to the NICS and the Induced Magnetic Field: The Case of the E₁₂^{2−} Spherenes (E = Ge, Sn, Pb), *J. Chem. Theory Comput.*, 2010, **6**(9), 2701–2705, DOI: [10.1021/ct100304c](https://doi.org/10.1021/ct100304c).
- 104 M. Orozco-Ic, J. Barroso, R. Islas and G. Merino, Delocalization in Substituted Benzene Dications: A Magnetic Point of View, *ChemistryOpen*, 2020, **9**(6), 657–661, DOI: [10.1002/open.202000105](https://doi.org/10.1002/open.202000105).
- 105 J. Vicha, M. Straka, M. L. Munzarová and R. Marek, Mechanism of Spin–Orbit Effects on the Ligand NMR Chemical Shift in Transition-Metal Complexes: Linking NMR to EPR, *J. Chem. Theory Comput.*, 2014, **10**(4), 1489–1499, DOI: [10.1021/ct400726y](https://doi.org/10.1021/ct400726y).
- 106 L. Alvarez-Thon and W. Caimanque-Aguilar, Spin-Orbit Effects on Magnetically Induced Current Densities in the



- M_4^{2-} (M = B, Al, Ga, In, Tl) Clusters, *Chem. Phys. Lett.*, 2017, **671**, 118–123, DOI: [10.1016/j.cplett.2017.01.027](https://doi.org/10.1016/j.cplett.2017.01.027).
- 107 A. E. Kuznetsov and A. I. Boldyrev, Theoretical Evidence of Aromaticity in X_3^- (X = B, Al, Ga) Species, *Struct. Chem.*, 2002, **13**(2), 141–148, DOI: [10.1023/A:1015704515336](https://doi.org/10.1023/A:1015704515336).
- 108 X. Chen, T. T. Chen, W. L. Li, J. B. Lu, L. J. Zhao, T. Jian, H. S. Hu, L. S. Wang and J. Li, Lanthanides with Unusually Low Oxidation States in the PrB_3^- and PrB_4^- Boride Clusters, *Inorg. Chem.*, 2019, **58**(1), 411–418, DOI: [10.1021/acs.inorgchem.8b02572](https://doi.org/10.1021/acs.inorgchem.8b02572).
- 109 M. Zhou, L. Andrews, J. Li and B. E. Bursten, Reaction of Laser-Ablated Uranium Atoms with CO: Infrared Spectra of the CUO, CUO^- , OUCCO, $(\eta^2-C_2)UO_2$, and $U(CO)_x$ ($x = 1-6$) Molecules in Solid Neon, *J. Am. Chem. Soc.*, 1999, **121**(41), 9712–9721, DOI: [10.1021/ja9921322](https://doi.org/10.1021/ja9921322).
- 110 J. Su, S. Hu, W. Huang, M. Zhou and J. Li, On the Oxidation States of Metal Elements in MO_3^- (M=V, Nb, Ta, Db, Pr, Gd, Pa) Anions, *Sci. China Chem.*, 2016, **59**(4), 442–451, DOI: [10.1007/s11426-015-5481-z](https://doi.org/10.1007/s11426-015-5481-z).
- 111 Y. Zheng, C.-S. Cao, W. Ma, T. Chen, B. Wu, C. Yu, Z. Huang, J. Yin, H.-S. Hu, J. Li, W.-X. Zhang and Z. Xi, 2-Butene Tetraanion Bridged Dinuclear Samarium(III) Complexes via Sm(II)-Mediated Reduction of Electron-Rich Olefins, *J. Am. Chem. Soc.*, 2020, **142**(24), 10705–10714, DOI: [10.1021/jacs.0c01690](https://doi.org/10.1021/jacs.0c01690).
- 112 Y. Xiao, X.-K. Zhao, T. Wu, J. T. Miller, H.-S. Hu, J. Li, W. Huang and P. L. Diaconescu, Distinct Electronic Structures and Bonding Interactions in Inverse-Sandwich Samarium and Ytterbium Biphenyl Complexes, *Chem. Sci.*, 2021, **12**(1), 227–238, DOI: [10.1039/D0SC03555F](https://doi.org/10.1039/D0SC03555F).

